


Research Article

Refertilization of Mantle Peridotites from the Central Indian Ridge: Response to a Geodynamic Transition

A. Hazra ^{1,2} A. Saha ¹ A. Verencar ¹ M. Satyanarayanan ³ S. Ganguly ²
and M. Kotha ²

¹CSIR-National Institute of Oceanography, Dona Paula, Goa 403004, India

²School of Earth, Ocean and Atmospheric Sciences, Goa University, Taleigão Plateau, Goa 403206, India

³CSIR-National Geophysical Research Institute, Uppal Road, Hyderabad 500007, India

Correspondence should be addressed to A. Saha; asaha.nio2015@gmail.com

Received 31 May 2021; Accepted 14 July 2021; Published 5 September 2021

Academic Editor: Koushik Sen

Copyright © 2021 A. Hazra et al. Exclusive Licensee GeoScienceWorld. Distributed under a Creative Commons Attribution License (CC BY 4.0).

The phenomena of reactive percolation of enriched asthenospheric melts and pervasive melt-rock interactions at mid oceanic ridge-rift systems are the principal proponents for mantle refertilization and compositional heterogeneity. This study presents new mineralogical and geochemical data for the abyssal peridotites exposed along the Vema and Vityaz fracture zones of the Central Indian Ridge (CIR) to address factors contributing to the chemical heterogeneity of CIR mantle. Cr-spinel (Cr#: 0.37–0.59) chemistry classifies these rocks as alpine-type peridotites and corroborates a transitional depleted MORB type to enriched, SSZ-related arc-type magma composition. HFSE and REE geochemistry further attests to an enriched intraoceanic forearc mantle affinity. The distinct boninitic signature of these rocks reflected by $LREE > MREE < HREE$ and PGE compositions substantiates refertilization of the CIR mantle harzburgites by boninitic melt percolation concomitant to initiation of oceanic subduction. The mineral chemistry, trace, and PGE signatures of the CIR peridotites envisage (i) replenishment of depleted sub-ridge upper mantle by impregnation of subduction-derived boninitic melts, (ii) tectonic transition from mid oceanic ridge-rift to an embryonic suprasubduction zone, and (iii) initiation of spontaneous intraoceanic subduction along submarine transform faults and fracture zones of slow-spreading CIR owing to the weakness and mechanical instability of older, denser, and negatively buoyant Indian Ocean lithosphere.

1. Introduction

The tectonic and magmatic processes contributing to the heterogeneous nature of the upper mantle posit important constraints on the composition and differentiation of the earth at various scales. Mid oceanic ridges (MOR) of intermediate, slow, and very slow spreading rates across the world's oceans are characterized by different crustal configurations portraying the compositional diversity of the upper mantle. The two viable processes that are attributed to chemical and isotopic heterogeneity of the mantle are: (i) multiple episodes of melt replenishment, melt-rock interaction, and mantle refertilization in open magma systems, and (ii) recycling of oceanic and continental crustal materials and components of subcontinental lithospheric mantle. Geochemical signatures of magmas in oceanic realms, owing to

minimal effects of contamination during ascent, record imprints of multiple episodes of melt replenishment, melt-rock interaction, fractional crystallization in open magma systems, and crustal recycling from paleotectonic events. These features provide a natural archive to probe into the compositional anomalies of the melting domains within the mantle. The mid oceanic ridge system (MOR) is a dynamic expression of the mantle convection cycle that governs the horizontal motion and interactions of lithospheric plates across the globe. Magmas generated at MORs form the oceanic crustal sequence by decompression melting of the upper mantle in response to plate divergence and hence render the upper mantle refractory in nature owing to successive melt extraction processes [1–3]. The oceanic crustal sequence consists of mid oceanic ridge basalts (MORB) including dykes, lower crustal cumulate gabbros, and peridotites,

whereas the serpentinized abyssal peridotites tectonically exhumed along the fracture zones, within transform faults, and locally exposed on rift valley floors at some slow-spreading ridges represent the residual upper mantle section of the oceanic lithosphere [4]. The geochemical and petrogenetic attributes of abyssal peridotites have yielded conspicuous evidence for the compositional diversity of suboceanic lithospheric mantle at divergent settings. Mantle heterogeneities from the global MOR systems have previously been addressed by researchers like Niu [4], Seyler et al. [5], and Brunelli et al. [6]. The chemical heterogeneities of the Indian Ocean MOR mantle have been propounded by Hellebrand et al. [7], Murton et al. [8], and Saha et al. [9].

This study presents petrology, mineral chemistry, bulk-rock major, trace, and PGE data for the abyssal mantle peridotites exposed along the Vema and Vityaz fracture zones of the northern portion (between 5 and 10°S) of the Central Indian Ridge (CIR) located in the Indian Ocean to address their petrogenetic evolution, geodynamic implications, and factors contributing to the refertilization of the Indian Ocean ridge mantle. The studied peridotites from the CIR represent the upper mantle section of the oceanic lithosphere tectonically exhumed on the ocean floor along the Vema and Vityaz transform faults and fracture zones. Therefore, the mineralogical and geochemical attributes of these mantle peridotites explicitly track the magmatic response to melt-percolation, melt-rock interaction, and mantle replenishment processes operative beneath the ridge system in an extensional tectonic regime.

2. Geological Background

The MOR system comprises about 70000 km long globe-encircling underwater continuous mountain chain of constructive plate boundary spreading throughout the major world oceans. The MORs have an average width of 300 km, rise up to ~2000 m above the seafloor, and constitute about 23% of the earth's surface [10]. The MORs are categorized into five types depending on the rate at which new crust is being created at the ridge axis: (a) ultraslow-spreading MOR with rate of full spreading < 20 mm/yr (e.g., Gakkel Ridge and Southwest Indian Ridge [11, 12]), (b) slow-spreading MOR with rate of full spreading between 20 and 40 mm/yr (e.g., Mid-Atlantic Ridge and Northern Central Indian Ridge [10]), (c) intermediate-spreading MOR with rate of full spreading 40-80 mm/yr (e.g., Juan de Fuca, Southern Central Indian Ridge, and Southeast Indian Ridge [13]), (d) fast-spreading MOR with rate of full spreading between 80 and 120 mm/yr (e.g., Northern East Pacific Rise [11]), and (e) ultrafast-spreading MOR with rate of full spreading between 120 and 160 mm/yr (e.g., Southern East Pacific Rise [11]). The CIR is a part of the Indian Ocean Ridge System (IORS) that includes four ridges; namely, Carlsberg (CR), Central Indian (CIR), Southwest Indian (SWIR), and Southeast Indian (SEIR) ridges. The CIR bifurcates at 25°30'S and 70°E at the Indian Ocean Triple Junction (IOTJ) in an apparently inverted Y shape to form SWIR and SEIR. The continuity of all these ridges is often offset by several NNE-SSW trending transform faults (also variously described as fracture zones), among which from north to

south—Owen, Mahabiss, Sealark, Vityaz, Vema, Argo, Marie Celeste, Egeria and Gemino, Prince Edward, Indomed, Amsterdam, and St. Paul—are of significance.

The present configuration of the Indian Plate evolved through diverse tectonothermal, geomorphological, and paleoclimatic conditions marked by supercontinent dispersal, seafloor spreading, birth of ocean basins, mantle plume activity, transform fault movements, subduction-accretion-collisional processes, and orogenic events during a 9000 km northward journey over 160 Ma time-frame. The breakup of Gondwana at 167 Ma and the Phanerozoic evolution of the Indian subcontinent with its adjacent ocean basins was predominantly influenced by the ongoing subduction of the Tethyan ocean floor beneath the southern margin of Eurasia [9, 14]. The Indian subcontinent got detached from the Gondwana supercontinent at 130 Ma and eventually amalgamated with the Eurasian supercontinent at 52 Ma. Thus, the opening of the Indian Ocean basin at 125 Ma and its subsequent evolutionary process were ubiquitously linked to the disintegration and drifting of African, Indian, Australian, Antarctic, and Arabian continental landmasses from the Gondwana supercontinent. The dispersal of Indian and African continental plates at 84 Ma led to the formation of the Northwest Indian Ocean that represents a potential zone to decipher ocean basin evolution, oceanic plate divergence, crustal accretion, propagation, and segmentation of ridges. Consequent to this, the movement of Africa towards west and separation of Australia and Antarctica around 53 Ma aided the northward journey of the Indian Plate and its collision with Eurasia at 50 Ma [14].

CIR is the northern arm of the Indian Ocean Ridge System (IORS) and extends approximately from latitude 2°S to 25°30'S and longitude from 62 to 67°E. At the Indian Ocean Triple Junction, the CIR bifurcates into two additional ridges such as the South East Indian Ridge (SEIR) and South West Indian Ridge (SWIR) [15, 16]. The CIR is about 2550 km long linear chain of active submarine volcanoes and tectonic regions, often displaced by numerous NNE-SSW trending transform faults and fracture zones [17]. The CIR is a slow- to intermediate-spreading ridge and seems to have attained its present geometry during the plate reorganization as a result of the Indian subcontinent colliding with Asia [18]. The formation of CIR is estimated about 38 Ma [19, 20] or the Late Cretaceous [17]. The present configuration of the Indian Ocean was attained by 36 Ma, and almost the entire Indian Ocean basin is <80 Ma old [14]. The interplay of tectonic and magmatic processes along the CIR significantly controls the oceanic crust generation, its thickness, and evolution of the oceanic core complexes (OCC) [21–25]. The CIR shows a typical morphology of a slow- (to intermediate) spreading ridge, having an axial valley of 500 to 1000 m deep. Kamesh Raju et al. [26] presented a 750 km long bathymetric map of CIR and demarcated the magmatic and less magmatic sections associating them with the transform faults and the nontransform discontinuities, respectively, and also confirmed the presence of megamulion structures along the aseismic less magmatic lineations on the CIR ocean floor. The axial volcanic ridges are around 1-2 km wide and up to 15 km in length. The general depth of

the ridge axis is around 3000 m; however, it increases up to 4000 m at the southernmost portion near the Rodrigues Triple Junction (RTJ) [8].

The NE-SW trending VMFZ (also known as Vema transform fault or fracture zone) right laterally offsets the NNW-SSE oriented CIR [27, 28]. The offset of the CIR has been variously estimated as 320 km [29], 300 km [30], and 240 km [31]. Detailed single and multibeam data found that the sea floor depth along the length of the VMFZ varies from 1500 to 6200 m [27, 28]. The principal transform displacement zone of the VMFZ consists of many closely spaced faults that can be traced for more than 150 km [32]. The mean full spreading rate of the CIR also varies between the ridge and segment located north of the VMFZ (3.6 cm/yr) and that to the south of the fracture zone (4.2 cm/yr). The segment north of the VMFZ displays intense deformation comprising alternating troughs (4800 m deep) and crests (2300 m). The average width of the CIR axial valley is about 15 km that varies from 12 km in the north to 17 km in the central part where it interacts with VMFZ [28]. The rock assemblage along VMFZ is very peculiar, consisting of both pillow and columnar basalts. The CIR is generally associated with smaller magma cells, displaying a characteristic low “bull's eye” Mantle Bouguer Anomaly (MBA) and gravity anomaly. This is in agreement with plume-like mantle upwelling and crustal density structure generally found along slow-spreading ridges [26]. The CIR segment to the north of VMFZ displays a well-defined, ridge-parallel topographic fabric. However, the southern segment appears to be undergoing a magmatic phase of accretion as understood from topographic fabric and rift valley morphology [26, 33]. Characterized, in general, by significantly low free air gravity anomalies, the VMFZ displays free air gravity anomalies to the order of 150 mGal [27]. It is maximum (200 mGal) at the steepest part of the transform fault [26, 33]. The VMFZ also shows a distinct seismicity pattern. It is characterized by low moment release (21.82×10^{25} dynes/cm) and low strain rate suggesting that a significant part of the plate motion in this segment is aseismic [34].

3. Materials and Methods

3.1. Sampling. The sampled rocks for this study were collected during the cruise SK-195 of the ORV Sagar Kanya. A total of nine dredge operations were made for the sampling of rocks on the ridge and fracture zones. These successful dredges recovered a variety of rocks ranging from basalts, gabbros, serpentinitized peridotites, ferromanganese encrusted rocks, and calcareous sediments. Studied serpentinitized peridotites were recovered from two dredges targeted at the fracture zones (Figure 1).

3.2. Analytical Techniques. The samples devoid of surface alteration were selected, and thin sections were prepared for optical microscopy. After petrographic studies, twelve (12) samples were selected for whole rock major oxides, trace elements and platinum group elements (PGE) analyses. Samples of around 1 kg were crushed and powdered to a

definite size (~120 mesh) using agate mortar to avoid contamination or loss of homogeneity at all stages.

The mineral chemical composition of the Cr-spinel, olivine, and orthopyroxene grains along with the serpentines was determined with CAMECA SX Five Electron Probe Micro Analyser at CSIR-National Institute of Oceanography (NIO), Goa, India. The analyses were performed with an acceleration voltage of 15 kV and beam current of 10 nA. Both natural mineral and synthetic standards were used during calibration. The precision of the analysis is better than 1% for major oxides from the repeated analyses of standards. Representative mineral chemical data are given in supplementary tables (Tables S1–S4).

Major oxide compositions were determined using X-ray fluorescence (XRF) spectrometer at CSIR-National Institute of Oceanography (NIO), Goa, India. Fusion beads of the powdered samples were used for the determination of major oxides by XRF. PANalytical's Axios WD, microprocessor controlled, sequential XRF covering the complete elemental range was used for the analyses of major oxides of representative rock samples. Certified reference materials BE-N and JP-1 were also analyzed along with the ultramafic rock samples to assess the accuracy of the data. Accuracy and precision are better than 5% RSD (% relative standard deviation).

Trace element compositions of representative whole rock samples were determined using High-Resolution Inductively Coupled Plasma Mass Spectrometer (HR-ICPMS) (Nu Instruments Attom®, UK) at CSIR-National Geophysical Research Institute (NGRI), Hyderabad, India. All rock samples were analyzed for a total of 34 trace elements including REE. A mixture of doubly distilled acids (HF:HNO₃) mixed in the ratio 7:3 was employed for the closed digestion method and the diluted solutions were analyzed by HR-ICPMS [35]. Certified reference materials UB-N (ANRT, France), PCC-1 (USGS, USA), and JP-1 (GSJ, Japan) [36] were used to validate the results obtained, and the precision for most of the elements was better than 5% RSD (% relative standard deviation).

Platinum group element concentrations were estimated by using the nickel sulphide fire-assay preconcentration method followed by High-Resolution Inductively Coupled Plasma Mass Spectrometer (HR-ICPMS) (Nu Instruments Attom®, UK) at CSIR-NGRI, Hyderabad, India. The analytical procedures of Balaram et al. [37] were followed during the digestion and analyses. Certified standards like WMG-1, WMS-1 (CANMET, Canada), and PTM-1 (IGGE, China) were used to check the quality of the analyses. The precision and reproducibility obtained for most of the platinum group of elements were better than 8% RSD.

4. Results

4.1. Petrography and Mineral Chemistry. The peridotites recovered from fracture zones of the Central Indian Ridge are highly altered and serpentinitized wherein at most of the places primary mineralogy is overprinted by hydrothermal alteration. The primary mineralogy of these peridotites is depicted by olivine, pyroxene, and opaque minerals. The olivine grains are altered to the serpentine group of minerals showing fibrous nature (Figure 2(a)). This serpentinitization

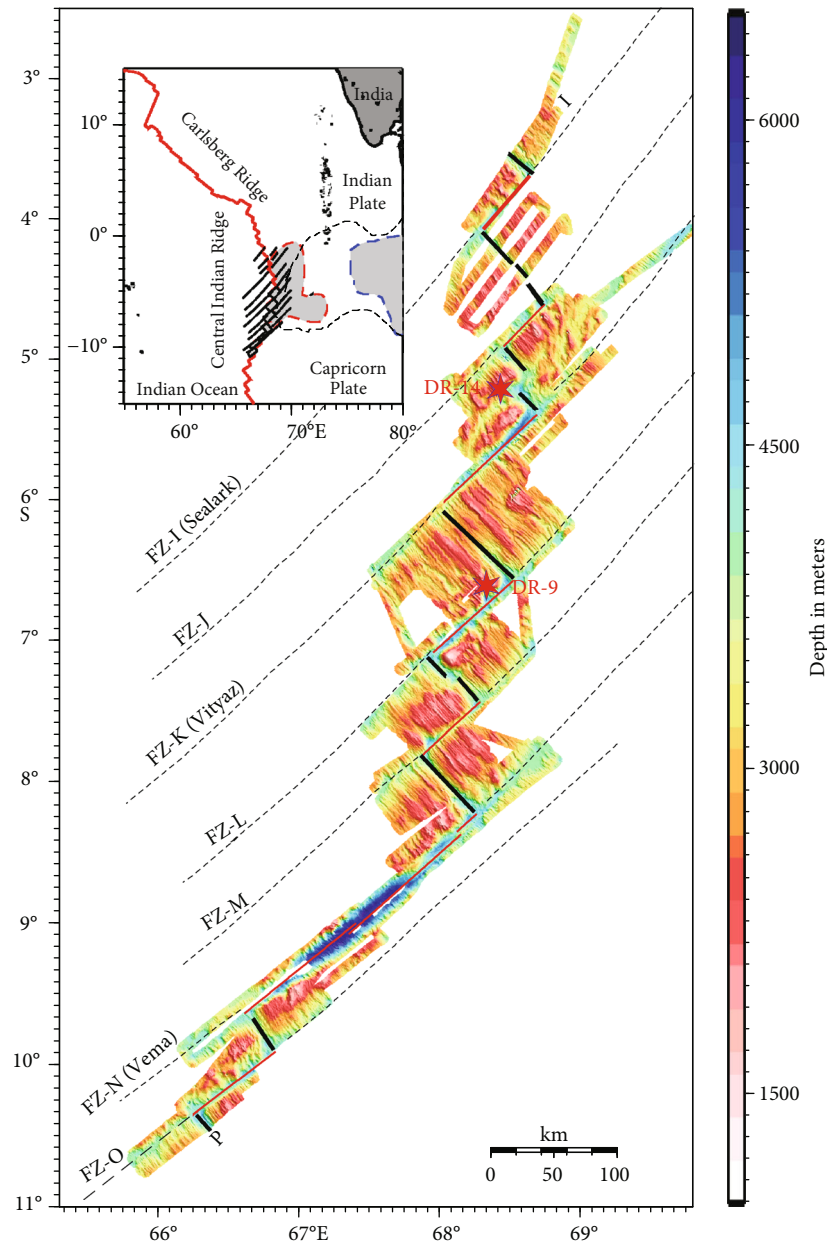


FIGURE 1: Multibeam bathymetry map of the study area. The dredge locations are represented by red stars in the bathymetric map of the study area [26]. Inset map shows the location of the Central Indian Ridge in the Indian Ocean Ridge System (IORS).

took place along the grain boundaries and cross fractures of olivine grains due to infiltration of sea-water and late-stage percolation of hydrothermal fluids (Figure 2(b)). In few places, relict olivine grains are also present (Figure 2(c)). Orthopyroxene is the second dominant mineral in these rocks (Figure 2(d)). In most places, pyroxene grains are also serpentinized, but the degree of alteration is much lesser than that in olivine. Clinopyroxene is also present in minor amounts. In these rocks, two types of opaque oxides are present. These opaques occur as primary magmatic minerals and as inclusions within the main rock forming silicates. Chromite and chromium-bearing spinels are the most dominant opaque phases present in these rocks. In the high-resolution microscopic study, the chromium-bearing spinels sometimes show

compositional zoning due to reaction failure at the time of their crystallization (Figure 2(e)). Apart from primary opaques, secondary Fe-rich opaques (~magnetites) are present, and these are products of alteration and formed mainly during late-stage hydrothermal activity (Figure 2(f)). These opaques occur along the secondary veins and grain boundary of olivine grains.

Serpentines from the studied samples are classified as antigorite and lizardite (Figure 3(a)). SiO₂ contents of these serpentines are almost similar to that of the other global serpentines and range from 34.73 to 44.93 wt.% (avg: 40.39 wt.%) and 26.04 to 45.49 wt.% (avg: 41.98 wt.%) for the mesh serpentines and vein serpentines, respectively (Table S1). MgO in both types ranges from 29.05 to 43.98 wt.% and 26.99 to 42.57 wt.%, respectively. Al₂O₃

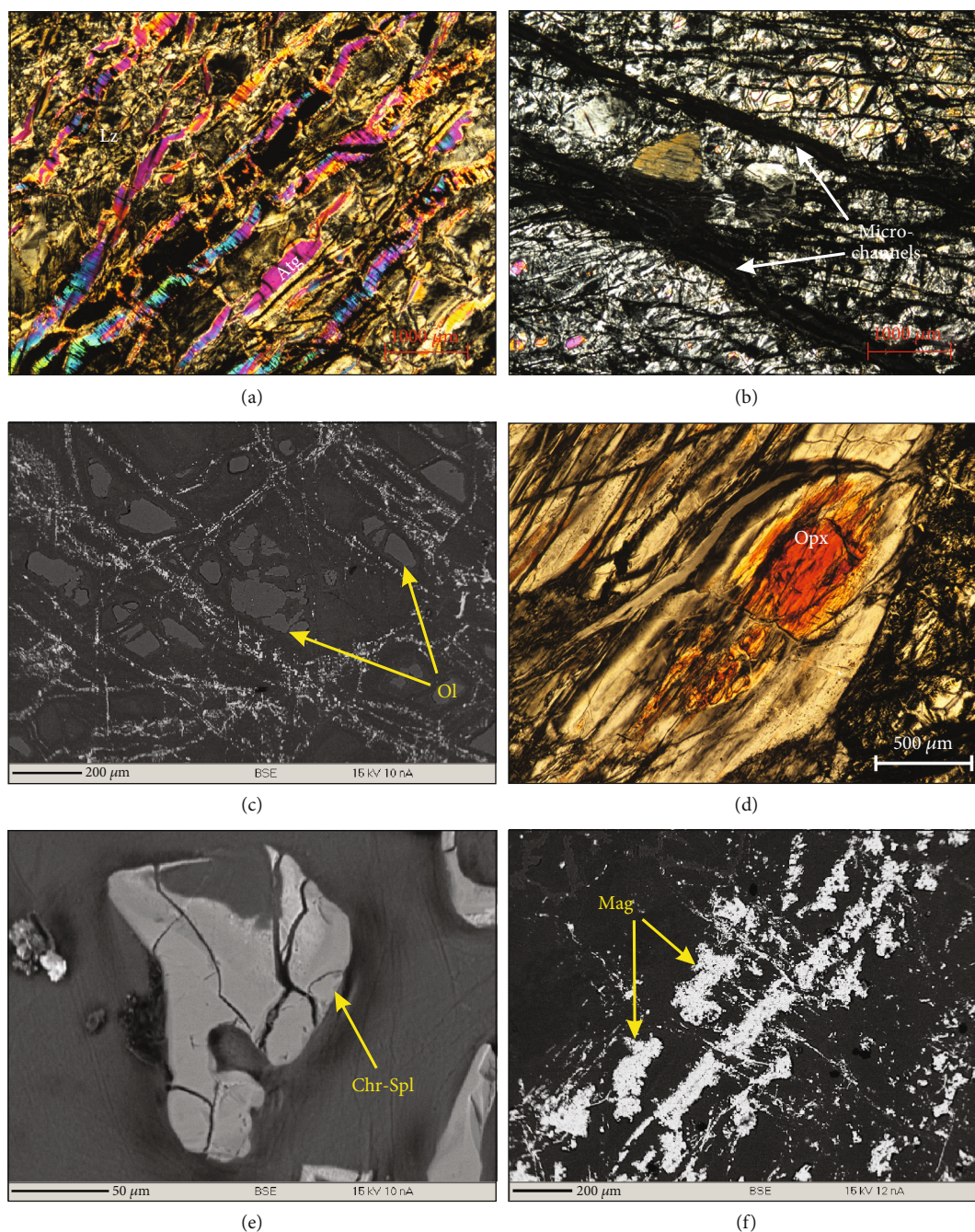


FIGURE 2: Photomicrographs showing (a) the occurrence of serpentine at the expense of olivine in serpentinized peridotites, (b) evidence of serpentinization along the grain boundaries, cross fractures of olivine grains due to sea-water interaction and late-stage percolation of hydrothermal fluid, (c) BSE image showing the presence of olivine grains, and (d) photomicrograph showing the presence of orthopyroxene grains in the studied mantle harzburgite. BSE image showing (e) the occurrence of chrome spinel and (f) secondary magnetite grains in the studied serpentinized peridotite.

content is also low (0.24 to 1.05 wt.%) for the vein serpentines, compared to that (0.08 to 3.69 wt.%) for the mesh serpentines. Antigorite is most stable at 680°C at 1.9 GPa, and the increase in Al and Cr in them expands the serpentinite stability by 60–70°C [38]. The higher Al and Cr contents of the antigorite of mesh serpentines relate to its greater stability in that temperature range. Average Mg# (Mg/Fe²⁺+Mg) values are 0.96 for the former and 0.95 for

the latter. These values do not correlate with the bulk rock compositions and are much higher thereby suggesting early crystallization of the precursor minerals in a distinct pressure-temperature condition.

The Cr-spinels from the restitic mantle peridotites of CIR are characterized by 22.8 to 45.6 wt.% Cr₂O₃ with high MgO content (5.44 to 17.32 wt.%) (Table S2). The high Al₂O₃ content of spinels ranging from 18.7 to 34.8 wt.% suggests

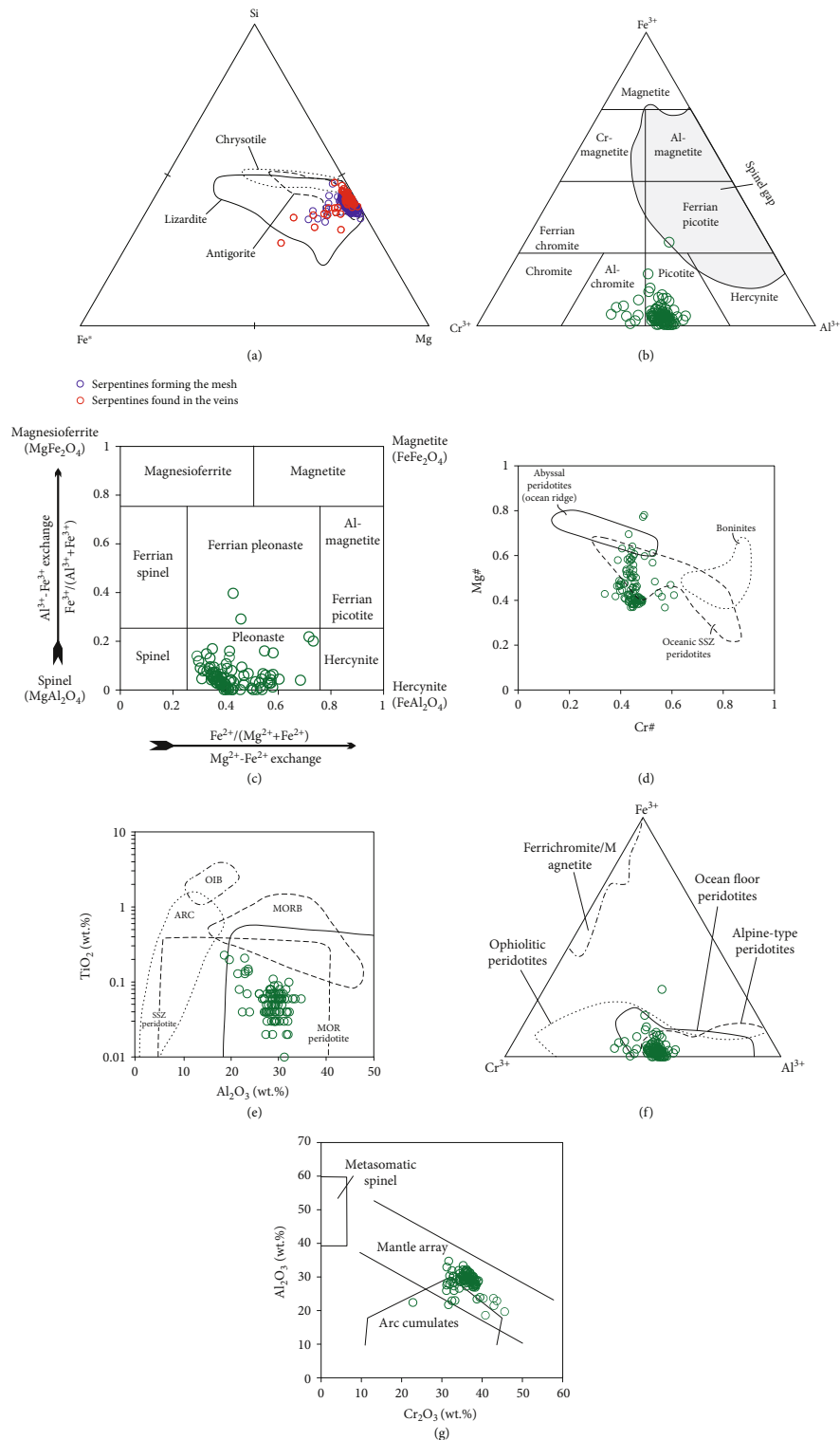


FIGURE 3: (a) Si-Fe-Mg plot showing the studied serpentines in the overlapping compositional domains for chrysotile, lizardite, and antigorite (fields for lizardite, chrysotile, and antigorite were compiled by D'Antonio and Kristensen [39]). (b) Cationic Fe-Cr-Al triangular diagram classifying the studied spinel as Al-chromite and picotite (c) in terms of Al-Fe and Mg-Fe exchange relations, the studied spinel corresponds to pleonaste composition (b, c, after Barnes and Roeder [40]). (d) Mg# vs. Cr# plots for analyzed spinel grains (fields after Cabanes and Mercier [41]). Most of the spinel grains are falling in the oceanic SSZ peridotite field, (e) TiO₂ vs. Al₂O₃ diagram for analyzed spinel grains shows a shift toward SSZ peridotites from MOR peridotites (fields of SSZ and MORB peridotites are from Kamenetsky et al. [42] and Rollinson [43]), and (f) spinel chemistry of studied peridotites is showing an affinity towards ocean floor peridotite (after Stevens [44]). Fields of peridotites are from Cookenboo et al. [45]. (g) Al₂O₃ vs. Cr₂O₃ plots for the studied spinel straddling the mantle and arc domains (after Franz and Wirth [46]).

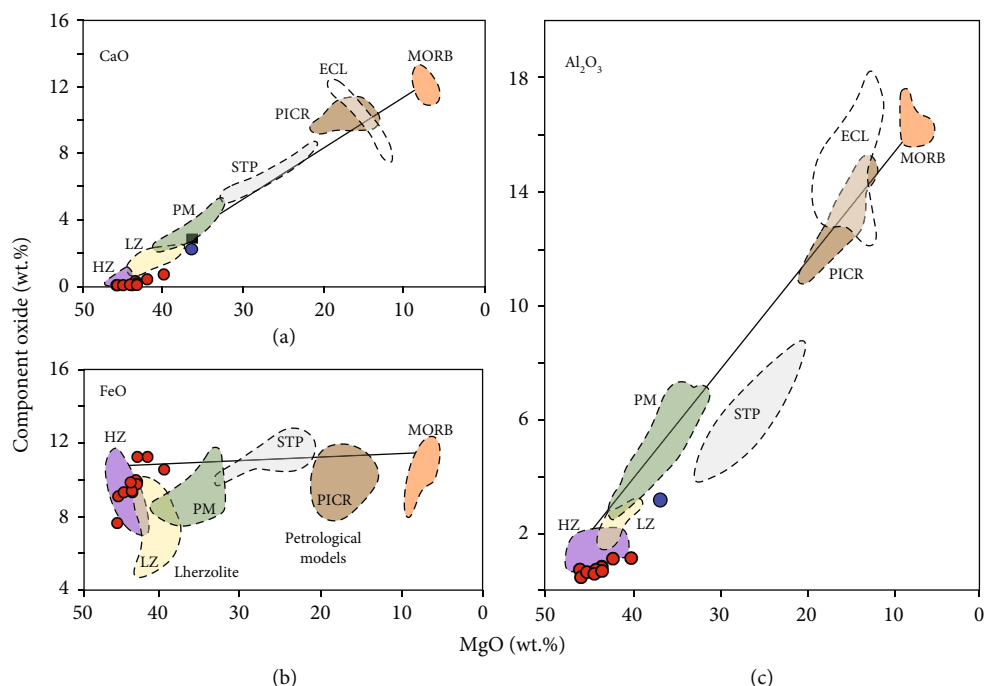


FIGURE 4: Plots of (a) CaO, (b) FeO, and (c) Al₂O₃ versus MgO for the studied CIR peridotites showing their harzburgitic nature. Fields after Anderson [49]. PM: primitive mantle; HZ: harzburgite; LZ: lherzolite; STP: spinifex textured komatiites; MORB: midoceanic ridge basalts; PICR: picrite.

its aluminous nature. The wide variation of Cr# (Cr/Cr+Al; molar ratio), ranging between 0.37 and 0.59 (<0.60; except one 0.61) indicates their affinity towards oceanic crust [47] (Table S2). Mineral chemical compositions characterize the chrome-spinels as Al-chromite, picotite, and pleonaste (Figures 3(b) and 3(c)). The chrome-spinel for the CIR mantle peridotite samples reflects transitional character from depleted MORB to an enriched SSZ regime in terms of Mg# vs. Cr# (Figure 3(d)) and TiO₂ vs. Al₂O₃ (Figure 3(e)) variations. The studied chrome-spinels largely correspond to the overlapping domain of ocean floor and alpine-type peridotites on a cationic Fe-Cr-Al diagram (Figure 3(f)) thereby corroborating the role of a subduction-related arc component. This conjecture is substantiated by their prominent arc signatures as reflected by the Al₂O₃ vs. Cr₂O₃ (Figure 3(g)) plot.

The olivine and orthopyroxene grains of the studied samples are extensively serpentinized. In few places, olivine and orthopyroxene pseudomorphs occur as relict. Few relict olivine and orthopyroxene grains are found suitable for mineral chemical analyses (Tables S3 and S4). Olivine grains are highly magnesian (avg: Fo_{~90}) in nature. Orthopyroxene chemistry (Wo_{4.7}En_{86.3}Fs₉) shows enstatitic composition. Single pyroxene thermometry [48] (figure not shown) indicates an equilibration temperature of ~1000-1400°C, thereby indicating that the peritectic reactions of Cr-spinels to form orthopyroxenes started at a high temperature regime, probably at crust-mantle transition zone.

4.2. Whole Rock Geochemistry. Major oxide compositions for the studied mantle peridotites (Table S5) reveal a restricted

SiO₂ content ranging from 37.5 to 40.84 wt.% with elevated abundances of MgO (35.42-39.45 wt.%). Al₂O₃ (0.02-0.42 wt.%), TiO₂ (0.4-0.97 wt.%), CaO (0.05-0.35 wt.%), and MnO (0.07-0.21 wt.%) characteristically show low concentrations with moderate values for Fe₂O₃^(t) (7.32-10.75 wt.%). Mg# varies largely from 74 to 82, attributing to the Mg-loss phenomena. CaO, FeO, and Al₂O₃ variations with respect to MgO classify the studied samples as harzburgites (Figures 4(a)-4(c)). They are characterized by high concentrations of Ni (1160-2084 ppm) and Cr (2158-2990 ppm) (Table S5). Chondrite-normalized REE patterns (Figure 5(a)) exhibit a U-shaped profile marked by pronounced LREE and HREE enrichment over MREE complying with La/Sm_N: 1.47-3.30, Dy/Yb_N: 0.40-0.91, and Gd/Yb_N: 0.53-1.53 (Table S5). Positive chondrite-normalized Eu anomalies (Figure 5(a)) suggest a plagioclase free source. LREE/MREE > 1 in conjunction with MREE/HREE < 1 reflects boninitic signatures of these rocks which in turn conform to subduction-derived melt percolation in the depleted ridge mantle. The primitive mantle-normalized trace element abundances (Figure 5(b)) display marked positive anomalies at U and negative anomalies at Nb.

The CIR mantle peridotites display moderate to high concentrations of total PGE (26.14-113.40 ppb) in which Pt concentration ranges from 9 to 29.37 ppb, Pd varies between 4.95 and 27.48 ppb, and Rh shows a range of 0.24-1.11 ppb among PPGE (Table S5). Among IPGE, Ir, Os, and Ru concentrations range from 2.76 to 15.06 ppb, 0.35-4.78 ppb, and 3.39-15.37 ppb, respectively. PGE abundances of the studied samples are marked by PPGE (18.83-76.28 ppb) enrichment relative to IPGE (7.31-37.12) (Table S5).

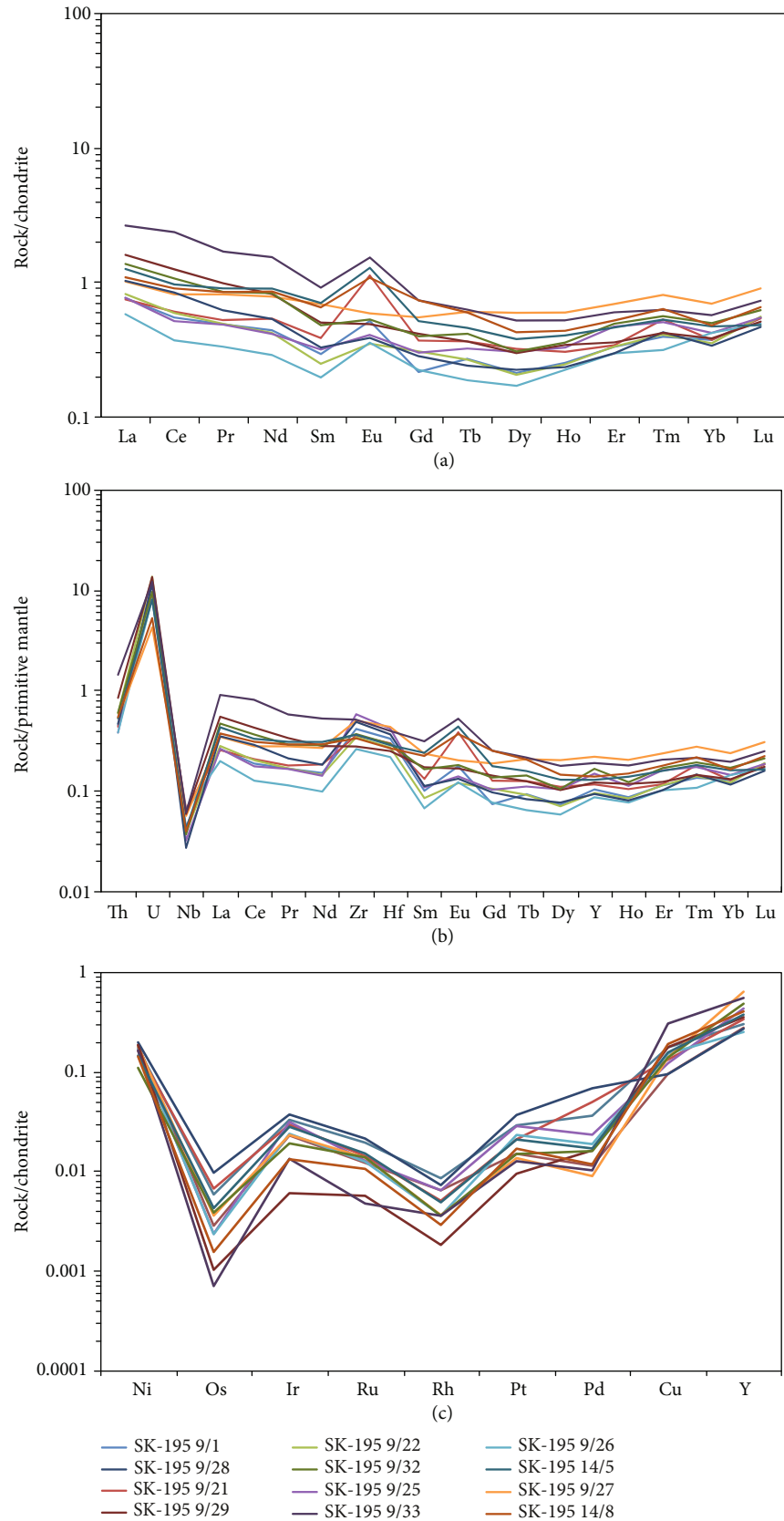


FIGURE 5: (a) Chondrite normalized REE, (b) primitive mantle (PM) normalized multi-element, and (c) chondrite normalized PGE diagrams for studied peridotites. For (a) and (b), normalization values are from Sun and McDonough [50], and for (c), normalization values are from McDonough and Sun [51].

Chondrite-normalized PGE patterns of CIR mantle peridotites (Figure 5(c)) are marked by a relative enrichment in Ir, Ru, Pt, Pd, and Cu and depletion in Os and Rh. These rocks have Pd/Ir (0.47–3.26) and Pd/Pt (0.36–1.3) (Table S5) ratios higher than those of primitive mantle (Pd/Ir: 1.01; Pd/Pt: 0.53) and chondrite (Pd/Ir: 1.0; Pd/Pt: 0.53).

5. Discussion

5.1. Screening for Alteration. The diverse thermotectonic conditions imprinted on peridotitic rocks of oceanic setting result in redistribution of elements through time via various post magmatic processes including hydrothermal alterations, metamorphism and related deformation, late-stage intrusions, metasomatic alterations, and carbonation [52–55]. Hence, identification of the primary geochemical characters is a prerequisite to address the petrogenesis and geodynamic implications of mantle peridotitic rocks. Chemistry of primary minerals comprises one of the most reliable proxies to understand the genesis and parent melt characters. Several studies have demonstrated that major elements like Al, Ti, Fe, and P, high field strength elements (HFSEs), REEs (except Eu and Ce), and transition metals like Cr, Ni, Sc, V, and Y are relatively immobile during hydrothermal alteration and greenschist to amphibolite grade metamorphism [56, 57]. Bulk major oxide chemistry of the peridotitic protolith remains unchanged by serpentinization and low grade metamorphism [53]. Peltonen et al. [58] demonstrated that transition metals like Sc, V, Cr, Co, and Ni are concentrated in early crystallizing mineral phases in the magma and suffer minimal fractionation, and they preserve the protolith signature in serpentinized peridotites. In this view, primary mineral chemistry, some of the major oxides, HFSEs, transition metals, and REE chemistry of whole rocks are used to decipher the petrogenetic processes and geodynamic conditions for the CIR peridotites in this study. None of the elements is showing any linear relationship with increasing LOI content of the studied samples nullifying the possibility of their mobility with the post magmatic serpentinization processes. Bulk rock PGE chemistry has been evaluated to underpin the mantle processes and melt generation mechanisms since IPGEs (Os, Ir, and Ru) are refractory in their behavior, unaffected by post magmatic alterations, and overall PPGE/IPPE is controlled by primary partial melting conditions, degree of melt percolation, and metasomatic processes in the mantle [59, 60].

5.2. Mantle Refertilization at Subduction Initiation. Global geochemical correlations of MORB invoke a complex interplay of magmatic and tectonic processes including variations in mantle temperature, degree of melting, rate of magma supply, and oceanic plate divergence involved in the generation of oceanic lithosphere at midoceanic ridge-rift systems with preponderant control on the crustal thickness and axial depth of the magma chamber beneath the ridge [61, 62]. The ascent and subsequent cooling of melts, resultant of decompression melting of asthenospheric mantle upwelling below midoceanic ridges, form the oceanic crust broadly

comprising 0.5 km thick MORB successively underlain by ~1.5 km of sheeted dykes and 4 to 5 km of cumulate gabbros with ultramafic rocks, while the residual melts form the depleted, refractory upper mantle [62–64]. The crustal and mantle sections of the oceanic lithosphere at midoceanic ridge-rift settings record different stages of elemental depletion or enrichment of subridge mantle through melt extraction and mantle refertilization mechanisms, respectively [65]. Mantle peridotites are generally envisaged to represent solid residues left after variable extents of melt extraction during oceanic crust formation. Consequently, the compositional variations reflected by these mantle relicts constrain the geodynamic conditions, magmatic episodes, partial melting, melt migration, and melt-rock interactions [66, 67]. Likewise, the peridotitic upper mantle section uplifted and exposed at Vema and Vityaz fractures zones of CIR provide a window to probe into the chemical heterogeneity of the Indian Ocean subridge upper mantle. The LILE, HFSE, and REE geochemistry reflects a deviation from typical, depleted N-MORB composition to an enriched intraoceanic forearc mantle further substantiating melt transfer from enriched asthenosphere to depleted lithospheric mantle and refertilization of the upper mantle peridotite by reactive melt percolation and melt-peridotite interactions [64, 68]. The compositional traits and elemental variations for the chrome-spinel from the CIR peridotites correspond to the overlapping domains of abyssal MOR peridotites and oceanic arc-related SSZ peridotites. Cr# ranging from 0.38 to 0.59 (except one data) for the chromian spinels in the studied abyssal peridotites from CIR classifies them as type I alpine-type peridotites thereby fingerprinting an evolving mantle character from MORB to a boninitic compositional trend [47]. Further, these mantle harzburgites with chromian spinels having Cr# > 30 conform to melt infiltration and melt-peridotite interaction [69]. The chrome-spinel chemistry (Figures 3(e) and 3(f)) for the studied samples implies a compositional transition from depleted MOR to a hydrated and enriched SSZ regime. The SSZ affinity for the studied samples can be equated with an intraoceanic forearc mantle wedge developed in response to incipient subduction. Multiple phases of melting, melt percolation, impregnation, and mantle refertilization under extensional conditions are potential indicators for a tectonic transition from ridge-rift to spontaneous subduction [70]. The mantle harzburgites exposed at Vema and Vityaz fracture zones of CIR record multiple stages of melting and refertilization as implicated by (i) ridge-associated melting rendering depleted upper mantle harzburgites and (ii) fluid-fluxed melting of juvenile forearc mantle triggering melt impregnation, melt-peridotite reaction, and refertilization of refractory peridotites. The evolved and enriched composition of oceanic mantle peridotites and their deviation from a typical N-MORB type DMM chemistry can be ascribed to (i) infiltration of plume-derived melts of OIB chemistry into a MOR magma chamber inducing incompatible trace element enrichment in the case of the proximity of ridge segments to plumes, (ii) subduction and recycling of OIB-like pyroxenite, (iii) refertilization of depleted subridge mantle by impregnation of subducted slab fluids and melts in the case of distal relation between plume and ridge at

the onset of spontaneous subduction at ridge transform faults, and (iv) melt replenishment in upwelling heterogeneous mantle by melting of residual eclogite derived from recycled oceanic crust [64, 68, 71, 72]. The CIR peridotites in this study yield unequivocal evidence for the compositional inhomogeneity of the Indian Ocean subridge mantle marked by interaction between depleted and enriched melt components. The absence of primitive mantle-normalized positive Nb anomalies coupled with extreme LREE enrichment over MREE and HREE discards the possibility of infiltration of OIB-type mantle components carried by plume-derived melts or recycled subducted slab materials into the refractory mantle beneath CIR. Rather, selective abundance of fluid-mobile elements (FME), HFSE depletion, and U-shaped chondrite-normalized REE patterns corroborate input from subduction-derived fluids and melts. The Nb/Zr vs. Th/Zr plot (Figure 6(a)) distinctly substantiates the fluid-related enrichment for the studied samples.

Higher values of Zr/Hf (avg: 45.16) and Zr/Sm (avg: 73.78) in addition to lower Nb/Ta (avg: 4.75) with respect to primitive mantle compositions (Zr/Hf: 36.25, Zr/Sm: 25.23, and Nb/Ta: 17.39) conform to a metasomatized, enriched mantle signature. Lower Nb/U (avg: 0.19) values with higher Ba/Th (avg: 213.16) and Ba/Nb (avg: 316.27), compared to OIB (Nb/U: 47.06, Ba/Th: 87.5, and Ba/Nb: 7.29) and N-MORB (Nb/U: 49.57, Ba/Th: 52.5, and Ba/Nb: 2.7), attest to contributions from subduction-derived fluids. The role of a recycled arc mantle could have been propounded as a key factor accounting for the enriched geochemical features of CIR mantle peridotites. However, the boninitic compositions of these rocks reflected on the V vs. Ti plot (Figure 6(b)) attest to melt input via melting of a juvenile, metasomatized forearc mantle during initiation of intraoceanic subduction. In general, boninite melt generation marks the compositional transition from anhydrous, depleted to hydrous, enriched mantle triggered by progressive influx of slab-derived fluids and melts during the nascent stage of oceanic subduction. The studied samples preserve ubiquitous signatures of boninitic melt-harzburgite interactions subsequent to spontaneous subduction initiation, generation, and infiltration of boninitic melts into the depleted mantle. The CIR mantle harzburgites reflect a geochemical and geodynamic transition from MOR to a SSZ regime developed in response to incipient subduction, and these mantle units constitute a geochemical record of mantle refertilization beneath CIR and melt-harzburgite interaction in a juvenile subduction-modified mantle. PGE chemistry marked by an abundance of PPGE over IPGE attests to infiltration of metasomatized, subduction-processed enriched components into depleted upper mantle. Pd/Ir vs. Ni/Cu variations for the studied samples (Figure 6(c)) conform to a mantle origin, while the Pd vs. Cu plot (Figure 6(d)) distinctly corroborates a sulphur undersaturated boninitic affinity. (Pt/Ir)_N vs. Cu (Figure 6(e)) variations display a melt percolation trend for the studied samples. Thus, these are infiltrated mantle peridotites pervasively impregnated by boninitic melts derived through juvenile forearc mantle melting in response to spontaneous subduction initiation at submarine transform faults and fracture zones in CIR. Subduction initiation marks the

first descent of oceanic lithosphere into the upper mantle prior to the inception of self-sustaining subduction. One of the primary triggers for this phenomenon comprises spontaneous sinking or gravitational collapse of older and denser oceanic lithosphere at transform faults and fracture zones [78–81]. Submarine transform faults and fracture zones are sites of pre-existing weakness or mechanical instability. Intraoceanic subduction zones can initiate along submarine transform faults and fracture zones and extensional detachment faults associated with slow- to ultraslow-spreading ridges [78, 82, 83]. Serpentinized oceanic detachments at midoceanic ridge-rift systems owing to their weak and fragile nature develop favorable conditions conducive for nucleation of incipient, spontaneous subduction parallel or close to spreading ridges [84]. This study infers the subduction initiation and prevalence of a juvenile, metasomatized forearc mantle associated with Vema and Vityaz fracture zones of CIR. This phenomenon generates boninitic melts that subsequently impregnate the depleted mantle peridotites. The Th_N vs. Nb_N plot (Figure 6(f)) substantiates the forearc affinity of the studied samples thereby corroborating the inception of spontaneous subduction beneath CIR. The serpentinized harzburgitic mantle sections exhumed at the transform fault sections of the CIR are potential archives of diverse magmatic features testifying to an evolving mantle composition from MORB to boninitic chemistry comparable to those developed in infant intraoceanic arc systems in response to multiple phases of fluid and melt impregnation associated with flux melting at initial stages of subduction [85, 86].

5.3. Implications for a Geodynamic Transition. Mantle sections of oceanic lithosphere at midoceanic ridge-rift settings are characteristically restitic or refractory in nature owing to multiple episodes of melt extraction and consequent impoverishment in incompatible trace elements. Thus, refractory mantle peridotites from which oceanic crust has been extracted at MOR exhibit an overall depleted chemistry with respect to primitive mantle and chondrite compositions [4, 87, 88]. However, MOR lithologies showing a deviation from this conventional depleted trend account for the geochemical heterogeneity of suboceanic mantle. Mantle refertilization and melt replenishment by subduction-derived melt percolation, plume-derived melt input, and episodic recycling of oceanic and continental crust are principal proponents for the chemical diversity of the upper mantle [88, 89]. These thermotectonic conditions render inevitable imprint on the mineralogical and whole rock geochemical compositions of oceanic crust and mantle lithologies [9, 68, 88, 90]. The unambiguous influence of mantle plume and recycled and stagnant subducted slabs on the composition of ridge mantle beneath oceanic spreading centers across the globe has been widely discussed [91]. One of the distinguishing features of the mantle peridotites exposed at the fracture zones of CIR, as inferred from the study, is the transitional geochemical and tectonic spectrum from depleted MOR to enriched SSZ. The distinct boninitic composition featured by the U-shaped chondrite-normalized REE patterns (Figure 7) for the studied CIR mantle harzburgites is not discernible for their crustal counterparts which

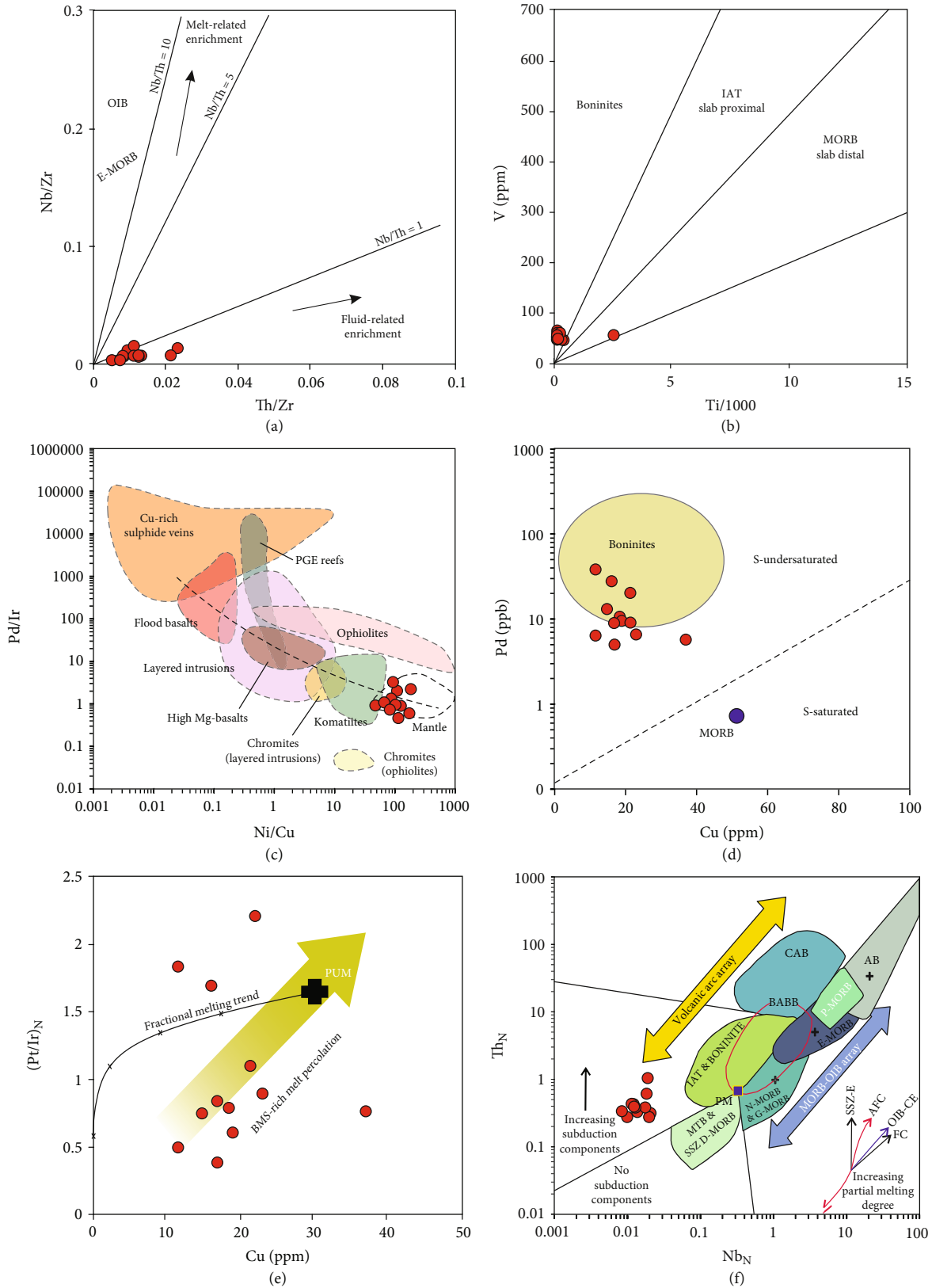


FIGURE 6: (a) Nb/Zr vs. Th/Zr plot showing the studied samples in an array consistent with fluid-related enrichment of mantle through the subduction process [73], (b) Ti vs. V plot attesting to the boninitic composition of the CIR mantle harzburgites [74], and (c) Pd/Ir vs. Ni/Cu diagram showing the plots for studied rocks occupying the field of mantle. Fields are after Barnes [75]. (d) Cu vs. Pd [76] plot showing sulphur undersaturated nature of CIR mantle peridotites, (e) $(Pt/Ir)_N$ vs. Cu plot for studied peridotites reflecting melt percolation, and (f) Th_N vs. Nb_N diagram [77] showing the forearc tectonic affinity for the studied samples.

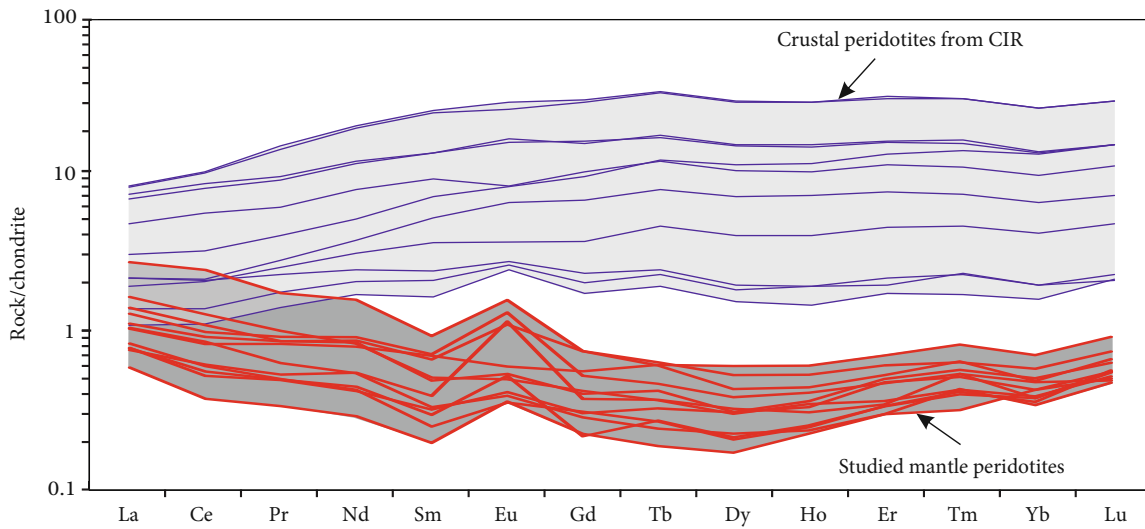


FIGURE 7: Chondrite normalized REE profiles for the studied mantle peridotites and crustal peridotites from CIR. Data of crustal peridotites are available from the authors.

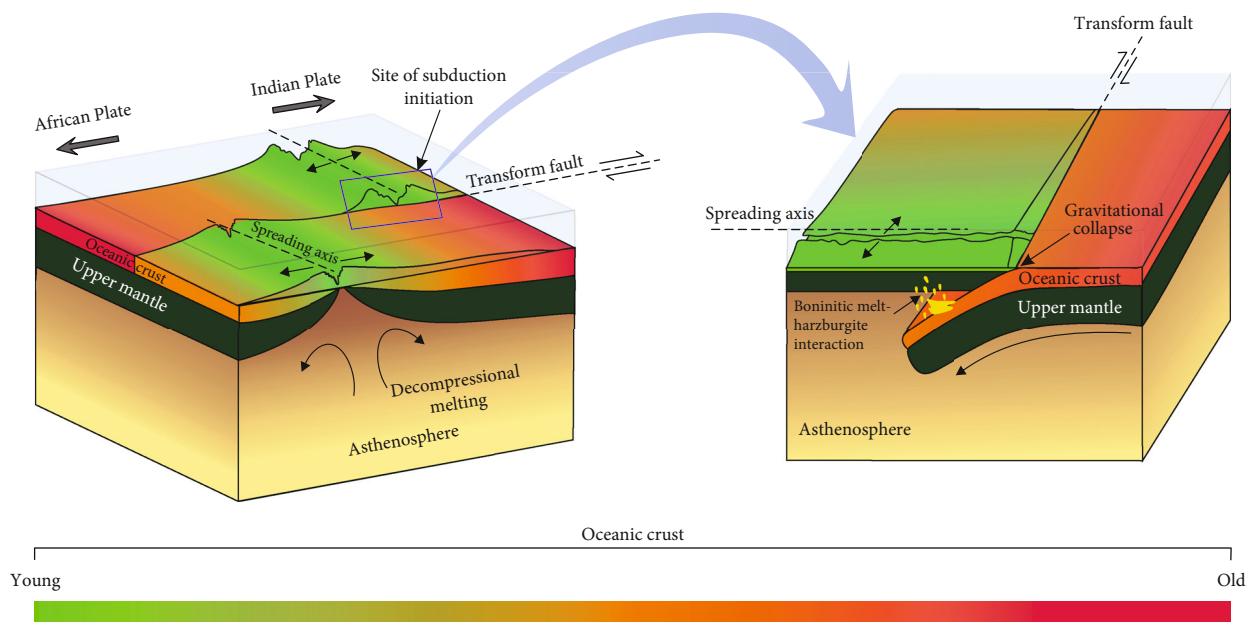


FIGURE 8: Schematic tectonic model showing spontaneous subduction initiation due to gravitational collapse of oceanic lithosphere along submarine transform faults at the Central Indian Ridge that ensued by refertilization of depleted mantle harzburgites through impregnation of boninitic melts.

exhibit typical LREE depleted MORB trend (Figure 7). This boninitic signature of the studied rocks, their forearc-related SSZ tectonic affinity (Figure 3(e)), and sulphur undersaturated nature (Figure 6(d)) as comprehensively revealed by mineral chemical compositions, whole rock, and PGE chemistry cannot be correlated with mantle plume activity or contributions from recycled/stagnant oceanic slab. Rather, the geochemical features inferred for the CIR peridotites can be validated in terms of a gradual transition in a magmatic and tectonic regime from decompression melting of a depleted lherzolitic mantle to fluid fluxed hydrous melting of fertile harzburgitic

mantle in response to inception of intraoceanic subduction. This progressive change is reflected in the melt generation process which is governed by combined effects of melt depletion and enrichment; mantle metasomatism and refertilization; and pervasive melt impregnation and melt-rock interactions. The favorable conditions for the generation of boninitic magmas include subduction of active spreading ridge or a young oceanic slab and initiation of spontaneous subduction along transform fault in an active ridge transform system. The depleted nature of the precursor mantle and unusual melting conditions involving elevated temperature and volatile influx at

shallow depth substantiate the transitional melt depletion and re-enrichment involved in boninite genesis [92, 93]. The dynamics of subduction initiation invokes two contrasting scenarios, where an older, denser, negatively buoyant oceanic lithosphere (at least 10 Ma old) subducts spontaneously into the underlying asthenosphere while the descent of younger (<1 Ma age), positively buoyant oceanic lithosphere requires external forces to initiate forced subduction [82]. A young, buoyant oceanic plate near a divergent boundary can only be forcefully subducted, whereas self-sustained, spontaneous subduction initiation is a more common phenomenon at mechanically weak zones associated with older and denser oceanic lithosphere. The magmatic response to this tectonic transition is imprinted within the lower oceanic crust and mantle sections in terms of elemental concentrations modified through pervasive melt-peridotite interactions. Thus in this case, spontaneous subduction initiation stands as the plausible proponent for the observed magmatic features of the relatively older and denser oceanic lithosphere existing away from the ridge axis at CIR (Figure 8). In coherence with this, the boninitization of CIR mantle peridotites can be interpreted to be linked with spontaneous subduction initiation at the fracture systems of CIR induced by gravitational collapse at the zones of lithospheric weakness and mechanical instability. Therefore, the mineral chemical, trace, and platinum group elemental signatures of the CIR mantle harzburgites collectively envisage the following: (i) replenishment of depleted subridge upper mantle by enriched subduction-derived melts and fluids indicates the role of a recycled arc mantle component or a tectonic transition from midoceanic ridge-rift to an embryonic suprasubduction zone, (ii) boninitic melt percolation underpins an incipient stage of oceanic subduction (Figure 8), and (iii) network of submarine transform faults and fracture zones along slow-spreading CIR owing to their weakness and mechanical instability develop favorable conditions to serve as potential precursors for initiation of spontaneous subduction (Figure 8) beneath Vema and Vityaz fracture zones of CIR.

6. Conclusion

- (i) Peridotites exposed at the Vema and Vityaz fracture zones of the Central Indian ridge-rift system represent a section of the Indian Ocean ridge mantle
- (ii) The geochemical attributes of the CIR peridotites mark a shift from MORB to arc signature that cannot be solely equated with the effects of serpentinization and hydrothermal alteration
- (iii) The absence of primitive mantle-normalized positive HFSE anomalies, $LREE > MREE < HREE$, and low Zr/Nb values collectively discarded the possibility of infiltration of low-degree plume-derived melts, OIB-type components, or recycled subducted slab materials and substantiate percolation of subduction-derived fluids and melts into the refractory mantle beneath the CIR
- (iv) The geochemical heterogeneities can be construed in terms of refertilization of depleted mantle by bonini-

tic melts generated through flux melting in response to spontaneous subduction initiation beneath CIR

- (v) Chrome spinel chemistry in conjunction with trace and PGE chemistry of the studied peridotite reconciles the phenomenon of boninitization of upper mantle beneath CIR and pervasive melt-peridotite interactions
- (vi) The fracture zones associated with CIR serve as a potential site for spontaneous subduction initiation owing to the weakness and mechanical instability of older, denser, and negatively buoyant oceanic lithosphere

Data Availability

All data have been provided in Supplementary Materials.

Conflicts of Interest

The authors do not report any conflicts of interest regarding the contents of this paper.

Acknowledgments

The authors are grateful to the Director of CSIR-National Institute of Oceanography for his encouragement, support, and permission to publish this work. The authors sincerely acknowledge all participating scientists and crew members of SK-195. The authors are thankful to Drs. K.A. Kameshraj, R. Mukhopadhyay, and S.D. Iyer for sharing the samples. The authors sincerely acknowledge the facilities received from Central Analytical Facility, CSIR-NIO. AS acknowledges the funding received from the Council of Scientific and Industrial Research (CSIR) and Ministry of Earth Sciences (MoES), Government of India, under MLP 2017 and GAP 2175, respectively. AH acknowledges CSIR for Senior Research Fellowship (Grant no. RF83931). This work is a part of Ph.D. of AH. This is NIO's contribution no. 6779.

Supplementary Materials

Table S1: EPMA data (in wt.%) of analyzed serpentines from the studied abyssal peridotites of the Central Indian Ridge. Table S2: EPMA data (in wt.%) of analyzed Cr-spinel grains from the studied abyssal peridotites of the Central Indian Ridge. Table S3: EPMA data (in wt.%) of analyzed olivine grains from the studied abyssal peridotites of the Central Indian Ridge. Table S4: EPMA data (in wt.%) of analyzed pyroxene grains from the studied abyssal peridotites of the Central Indian Ridge. Table S5: Major, trace, and PGE compositions of the studied abyssal peridotites from the Central Indian Ridge. (*Supplementary Materials*)

References

- [1] M. Seyler, M. Cannat, and C. Mevel, "Evidence for major-element heterogeneity in the mantle source of abyssal peridotites from the Southwest Indian Ridge (52° to 68°E)," *Geochemistry, Geophysics, Geosystems*, vol. 4, no. 2, 2003.

- [2] M. Seyler, J. P. Lorand, M. J. Toplis, and G. Godard, "Asthenospheric metasomatism beneath the mid-ocean ridge: evidence from depleted abyssal peridotites," *Geology*, vol. 32, no. 4, p. 301, 2004.
- [3] C. M. Meyzen, J. N. Ludden, E. Humler et al., "New insights into the origin and distribution of the DUPAL isotope anomaly in the Indian Ocean mantle from MORB of the Southwest Indian Ridge," *Geochemistry, Geophysics Geosystems*, vol. 6, no. 11, 2005.
- [4] Y. Niu, "Bulk-rock major and trace element compositions of abyssal peridotites: implications for mantle melting, melt extraction and post-melting processes beneath mid-ocean ridges," *Journal of Petrology*, vol. 45, no. 12, pp. 2423–2458, 2004.
- [5] M. Seyler, M. J. Toplis, J. P. Lorand, A. Luguët, and M. Cannat, "Clinopyroxene microtextures reveal incompletely extracted melts in abyssal peridotites," *Geology*, vol. 29, no. 2, p. 155, 2001.
- [6] D. Brunelli, M. Seyler, A. Cipriani, L. Ottolini, and E. Bonatti, "Discontinuous melt extraction and weak refertilization of mantle peridotites at the Vema lithospheric section (Mid-Atlantic Ridge)," *Journal of Petrology*, vol. 47, no. 4, pp. 745–771, 2006.
- [7] E. Hellebrand, J. E. Snow, P. Hoppe, and A. W. Hoffmann, "Garnet-field melting and late-stage refertilization in 'residual' abyssal peridotites from the Central Indian Ridge," *Journal of Petrology*, vol. 43, no. 12, pp. 2305–2338, 2002.
- [8] B. J. Murton, A. G. Tindle, J. A. Milton, and D. Sauter, "Heterogeneity in southern Central Indian Ridge MORB: implications for ridge-hot spot interaction," *Geochemistry, Geophysics, Geosystems*, vol. 6, no. 3, 2005.
- [9] A. Saha, S. Sensarma, A. Hazra et al., "Imprints of ancient recycled oceanic lithosphere in heterogeneous Indian Ocean mantle: evidence from petrogenesis of Carlsberg Ridge basalts from Northwest Indian Ocean," *Gondwana Research*, vol. 86, pp. 60–82, 2020.
- [10] S. D. Iyer, R. Mukhopadhyay, R. K. Drolia, and D. Ray, "Mid-ocean ridges, InRidge and the future," *Current Science*, vol. 85, no. 3, pp. 272–276, 2003.
- [11] E. P. Dubinin, A. V. Kokhan, and N. M. Sushchevskaya, "Tectonics and magmatism of ultraslow spreading ridges," *Geotectonics*, vol. 47, no. 3, pp. 131–155, 2013.
- [12] J. Son, S. J. Pak, J. Kim et al., "Tectonic and magmatic control of hydrothermal activity along the slow-spreading Central Indian Ridge, 8°S–17°S," *Geochemistry, Geophysics, Geosystems*, vol. 15, no. 5, pp. 2011–2020, 2014.
- [13] R. Mukhopadhyay, S. D. Iyer, D. Ray, S. M. Karisiddaiah, and R. K. Drolia, "Morphotectonic and petrological variations along the southern Central Indian Ridge," *International Journal of Earth Sciences*, vol. 105, no. 3, pp. 905–920, 2016.
- [14] S. Chatterjee, A. Goswami, and C. R. Scotese, "The longest voyage: tectonic, magmatic, and paleoclimatic evolution of the Indian Plate during its northward flight from Gondwana to Asia," *Gondwana Research*, vol. 23, no. 1, pp. 238–267, 2013.
- [15] E. Humler and H. Whitechurch, "Petrology of basalts from the Central Indian Ridge (lat. 25°23'S, long. 70°04'E): estimates of frequencies and fractional volumes of magma injections in a two-layered reservoir," *Earth and Planetary Science Letters*, vol. 88, no. 1–2, pp. 169–181, 1988.
- [16] D. Ray, S. Misra, and R. Banerjee, "Geochemical variability of MORBs along slow to intermediate spreading Carlsberg-Central Indian Ridge, Indian Ocean," *Journal of Asian Earth Sciences*, vol. 70, pp. 125–141, 2013.
- [17] S. D. Iyer and D. Ray, "Structure, tectonic and petrology of mid-oceanic ridges and the Indian scenario," *Current Science*, vol. 85, no. 3, pp. 277–289, 2003.
- [18] M. Radhakrishna and R. K. Verma, "Seismotectonics of the Central Indian Ridge, western Indian Ocean," *Journal of Geological Society of India*, vol. 55, pp. 515–527, 2000.
- [19] P. Patriat and J. Achache, "India-Eurasia collision chronology has implications for crustal shortening and driving mechanism of plates," *Nature*, vol. 311, no. 5987, pp. 615–621, 1984.
- [20] M. R. Fisk, R. A. Duncan, A. N. Baxter, J. D. Greenough, R. B. Hargraves, and Y. Tatsumi, "Reunion hotspot magma chemistry over the past 65 m.y.: results from Leg 115 of the Ocean Drilling Program," *Geology*, vol. 17, no. 10, p. 934, 1989.
- [21] K. C. Macdonald, P. J. Fox, L. J. Perram et al., "A new view of the mid-ocean ridge from the behaviour of ridge-axis discontinuities," *Nature*, vol. 335, no. 6187, pp. 217–225, 1988.
- [22] K. C. Macdonald, D. S. Scheirer, and S. M. Carbotte, "Mid-ocean ridges: discontinuities, segments and giant cracks," *Science*, vol. 253, no. 5023, pp. 986–994, 1991.
- [23] J. Lin, G. M. Purdy, H. Schouten, J. C. Sempere, and C. Zervas, "Evidence from gravity data for focused magmatic accretion along the Mid-Atlantic Ridge," *Nature*, vol. 344, no. 6267, pp. 627–632, 1990.
- [24] J. Lin and J. P. Morgan, "The spreading rate dependence of three-dimensional mid-ocean ridge gravity structure," *Geophysical Research Letters*, vol. 19, no. 1, pp. 13–16, 1992.
- [25] M. Tolstoy, A. J. Harding, and J. A. Orcutt, "Crustal thickness on the Mid-Atlantic Ridge: bull's-eye gravity anomalies and focused accretion," *Science*, vol. 262, no. 5134, pp. 726–729, 1993.
- [26] K. A. Kamesh Raju, K. Samudrala, R. K. Drolia, D. Amarnath, R. Ramachandran, and A. Mudholkar, "Segmentation and morphology of the Central Indian Ridge between 3°S and 11°S, Indian Ocean," *Tectonophysics*, vol. 554–557, pp. 114–126, 2012.
- [27] R. Mukhopadhyay, S. D. Iyer, and R. Batiza, "Petrology of seamounts in the Central Indian Ocean Basin: evidence for near-axis origin," *Geo-Marine Letters*, vol. 15, pp. 106–110, 1998.
- [28] R. K. Drolia, S. D. Iyer, B. Chakraborty et al., "The Northern Central Indian Ridge: geology and tectonics of fracture zones-dominated spreading ridge segments," *Current Science*, vol. 85, pp. 290–298, 2003.
- [29] W. M. White, "Sources of oceanic basalts: radiogenic isotopic evidence," *Geology*, vol. 13, no. 2, p. 115, 1985.
- [30] R. L. Fisher, J. G. Sclater, and D. P. McKenzie, "Evolution of the Central Indian Ridge, western Indian Ocean," *Geological Society of America Bulletin*, vol. 82, no. 3, p. 553, 1971.
- [31] C. DeMets, R. G. Gordon, and J. Y. Royer, "Motion between the Indian, Capricorn and Somalian plates since 20 Ma: implications for the timing and magnitude of distributed lithospheric deformation in the equatorial Indian Ocean," *Geophysical Journal International*, vol. 161, no. 2, pp. 445–468, 2005.
- [32] R. K. Drolia and C. DeMets, "Deformation in the diffuse India-Capricorn-Somalia triple junction from a multibeam and magnetic survey of the northern Central Indian Ridge, 3°S–10°S," *Geochemistry, Geophysics, Geosystems*, vol. 6, no. 9, 2005.
- [33] K. A. Kamesh Raju, A. V. Mudholkar, and K. Samudrala, "Slow spreading ridges of the Indian Ocean: an overview of marine

- geophysical investigations,” *Journal of Indian Geophysical Union*, vol. 19, pp. 137–159, 2015.
- [34] M. R. Krishna, “Seismic moment release along selected major transforms on the Central Indian Ridge, Western Indian Ocean, and its tectonic implications,” *Proceedings of the Indian Academy of Sciences-Earth and Planetary Sciences*, vol. 104, no. 4, pp. 693–706, 1995.
- [35] M. Satyanarayanan, V. Balaram, S. S. Sawant et al., “Rapid determination of REEs, PGEs, and other trace elements in geological and environmental materials by high resolution inductively coupled plasma mass spectrometry,” *Atomic Spectroscopy*, vol. 39, no. 1, pp. 1–15, 2018.
- [36] K. Govindaraju, “1994 Compilation of working values and sample description for 383 geostandards,” *Geostandards Newsletter*, vol. 18, no. 1, pp. 1–158, 1994.
- [37] V. Balaram, R. Mathur, V. K. Banakar et al., “Determination of the platinum–group elements (PGE) and gold (Au) in manganese nodule reference samples by nickel sulfide fire-assay and Te coprecipitation with ICP-MS,” *Indian Journal of Geo-Marine Sciences*, vol. 35, pp. 7–16, 2006.
- [38] J. A. Padrón-Navarta, J. Hermann, C. J. Garrido, V. López Sánchez-Vizcaíno, and M. T. Gómez-Pugnaire, “An experimental investigation of antigorite dehydration in natural silica-enriched serpentinite,” *Contributions to Mineralogy and Petrology*, vol. 159, no. 1, pp. 25–42, 2010.
- [39] M. D’Antonio and M. B. Kristensen, “Serpentine and brucite of ultramafic clasts from the South Chamorro Seamount (Ocean Drilling Program Leg 195, site 1200): inferences for the serpentinization of the Mariana forearc mantle,” *Mineralogical Magazine*, vol. 68, no. 6, pp. 887–904, 2004.
- [40] S. J. Barnes and P. L. Roeder, “The range of spinel compositions in terrestrial mafic and ultramafic rocks,” *Journal of Petrology*, vol. 42, no. 12, pp. 2279–2302, 2001.
- [41] N. Cabanes and J. C. C. Mercier, “Insight into the upper mantle beneath an active extensional zone: the spinel-peridotite xenoliths from San Quintin (Baja California, Mexico),” *Contributions to Mineralogy and Petrology*, vol. 100, no. 3, pp. 374–382, 1988.
- [42] V. S. Kamenetsky, A. J. Crawford, and S. Meffre, “Factors controlling chemistry of magmatic spinel: an empirical study of associated olivine, Cr-spinel and melt inclusions from primitive rocks,” *Journal of Petrology*, vol. 42, no. 4, pp. 655–671, 2001.
- [43] H. Rollinson, “The geochemistry of mantle chromitites from the northern part of the Oman ophiolite: inferred parental melt compositions,” *Contributions to Mineralogy and Petrology*, vol. 156, no. 3, pp. 273–288, 2008.
- [44] R. E. Stevens, “Composition of some chromites of the western hemisphere,” *American Mineralogist*, vol. 29, no. 1–2, pp. 1–34, 1944.
- [45] H. O. Cookenboo, R. M. Bustin, and K. R. Wilks, “Detrital chromian spinel compositions used to reconstruct the tectonic setting of provenance: implications for orogeny in the Canadian Cordillera,” *Journal of Sedimentary Research*, vol. 67, no. 1, pp. 116–123, 1997.
- [46] L. Franz and R. Wirth, “Spinel inclusions in olivine of peridotite xenoliths from TUBAF seamount (Bismarck Archipelago/Papua New Guinea): evidence for the thermal and tectonic evolution of the oceanic lithosphere,” *Contributions to Mineralogy and Petrology*, vol. 140, no. 3, pp. 283–295, 2000.
- [47] H. J. Dick and T. Bullen, “Chromian spinel as a petrogenetic indicator in abyssal and alpine-type peridotites and spatially associated lavas,” *Contributions to Mineralogy and Petrology*, vol. 86, no. 1, pp. 54–76, 1984.
- [48] D. H. Lindsley, “Pyroxene thermometry,” *American Mineralogist*, vol. 68, pp. 477–493, 1983.
- [49] D. L. Anderson, *Theory of the Earth*, Blackwell scientific publications, Hoboken, NJ, USA, 1989.
- [50] S. S. Sun and W. F. McDonough, *Chemical and isotopic systematics of oceanic basalts: implications for mantle composition and processes*, vol. 42, Geological Society, London, 1989.
- [51] W. F. McDonough and S. S. Sun, “The composition of the Earth,” *Chemical Geology*, vol. 120, pp. 223–253, 1995.
- [52] J. L. Bodinier and M. Godard, “Orogenic, ophiolitic, and abyssal peridotites,” *Treatise on Geochemistry*, vol. 2, p. 568, 2003.
- [53] F. Deschamps, M. Godard, S. Guillot, and K. Hattori, “Geochemistry of subduction zone serpentinites: a review,” *Lithos*, vol. 178, pp. 96–127, 2013.
- [54] Y. Xu, J. Liu, Q. Xiong et al., “The complex life cycle of oceanic lithosphere: a study of Yarlung-Zangbo ophiolitic peridotites, Tibet,” *Geochimica et Cosmochimica Acta*, vol. 277, pp. 175–191, 2020.
- [55] I. M. Bhat, T. Ahmad, D. S. Rao, S. Balakrishnan, and N. C. Rao, “PGE and isotopic characteristics of Shergol and Suru Valley ophiolites, Western Ladakh: implications for supra-subduction tectonics along Indus suture zone,” *Geoscience Frontiers*, vol. 12, no. 3, article 101118, 2021.
- [56] M. R. Laflèche, C. Dupuy, and H. Bougault, “Geochemistry and petrogenesis of Archean mafic volcanic rocks of the southern Abitibi Belt, Quebec,” *Precambrian Research*, vol. 57, no. 3–4, pp. 207–241, 1992.
- [57] N. Said, R. Kerrich, and D. Groves, “Geochemical systematics of basalts of the Lower Basalt Unit, 2.7 Ga Kambalda Sequence, Yilgarn craton, Australia: Plume impingement at a rifted craton margin,” *Lithos*, vol. 115, no. 1–4, pp. 82–100, 2010.
- [58] P. Peltonen, A. Kontinen, and H. Huhma, “Petrogenesis of the mantle sequence of the Jormua ophiolite (Finland): melt migration in the upper mantle during Palaeoproterozoic continental break-up,” *Journal of Petrology*, vol. 39, no. 2, pp. 297–329, 1998.
- [59] C. Manikyamba and A. Saha, “PGE geochemistry of komatiites from Neoproterozoic Sigegudda greenstone terrane, western Dharwar Craton, India,” *Geological Society of India Special Publication*, vol. 2, pp. 162–174, 2014.
- [60] A. Saha, C. Manikyamba, M. Santosh, S. Ganguly, A. C. Khelen, and K. S. V. Subramanyam, “Platinum group elements (PGE) geochemistry of komatiites and boninites from Dharwar Craton, India: implications for mantle melting processes,” *Journal of Asian Earth Sciences*, vol. 105, pp. 300–319, 2015.
- [61] F. Schmid, V. Schlindwein, I. Koulakov, A. Plötz, and J. R. Scholz, “Magma plumbing system and seismicity of an active mid-ocean ridge volcano,” *Scientific Reports*, vol. 7, no. 1, 2017.
- [62] P. Li, Q. K. Xia, L. Dallai et al., “High H₂O content in pyroxenes of residual mantle peridotites at a Mid Atlantic Ridge segment,” *Scientific Reports*, vol. 10, no. 1, 2020.
- [63] C. H. Langmuir, E. M. Klein, and T. Plank, “Petrological systematics of mid-ocean ridge basalts: constraints on melt generation beneath ocean ridges,” in *Mantle Flow and Melt Generation at Mid-Ocean Ridges*, J. P. Morgan, D. K.

- Blackman, and J. M. Sinton, Eds., vol. 71, pp. 183–280, *Geophysical Monograph Series*, American Geophysical Union, 1992.
- [64] H. Hao, I. H. Campbell, R. J. Arculus, and M. R. Perfit, “Using precious metal probes to quantify mid-ocean ridge magmatic processes,” *Earth and Planetary Science Letters*, vol. 553, article 116603, 2021.
- [65] L. Patkó, N. Liptai, L. E. Aradi et al., “Metasomatism-induced wehrlite formation in the upper mantle beneath the Nograd-Gomor Volcanic Field (Northern Pannonian Basin): Evidence from xenoliths,” *Geoscience Frontiers*, vol. 11, no. 3, pp. 943–964, 2020.
- [66] I. J. Parkinson and J. A. Pearce, “Peridotites from the Izu–Bonin–Mariana forearc (ODP Leg 125): evidence for mantle melting and melt–mantle interaction in a supra-subduction zone setting,” *Journal of Petrology*, vol. 39, no. 9, pp. 1577–1618, 1998.
- [67] E. Aldanmaz, D. J. van Hinsbergen, Ö. Yıldız-Yükseköl et al., “Effects of reactive dissolution of orthopyroxene in producing incompatible element depleted melts and refractory mantle residues during early fore-arc spreading: constraints from ophiolites in eastern Mediterranean,” *Lithos*, vol. 360–361, article 105438, 2020.
- [68] E. Rampone, G. Borghini, and V. Basch, “Melt migration and melt-rock reaction in the Alpine-Apenine peridotites: insights on mantle dynamics in extending lithosphere,” *Geoscience Frontiers*, vol. 11, no. 1, pp. 151–166, 2020.
- [69] S. K. Birner, E. Cottrell, J. M. Warren, K. A. Kelley, and F. A. Davis, “Melt addition to mid-ocean ridge peridotites increases spinel Cr with no significant effect on recorded oxygen fugacity,” *Earth and Planetary Science Letters*, vol. 566, article 116951, 2021.
- [70] M. Ulrich, C. Picard, S. Guillot, C. Chauvel, D. Cluzel, and S. Meffre, “Multiple melting stages and refertilization as indicators for ridge to subduction formation: the New Caledonia ophiolite,” *Lithos*, vol. 115, no. 1–4, pp. 223–236, 2010.
- [71] A. Rosenthal, G. M. Yaxley, D. H. Green, J. Hermann, I. Kovács, and C. Spandler, “Continuous eclogite melting and variable refertilisation in upwelling heterogeneous mantle,” *Scientific Reports*, vol. 4, 2014.
- [72] S. Yang, M. Humayun, and V. J. Salters, “Elemental constraints on the amount of recycled crust in the generation of mid-oceanic ridge basalts (MORBs),” *Science Advances*, vol. 6, no. 23, 2020.
- [73] J. H. Zhao and M. F. Zhou, “Geochemistry of Neoproterozoic mafic intrusions in the Panzhihua district (Sichuan Province, SW China): Implications for subduction-related metasomatism in the upper mantle,” *Precambrian Research*, vol. 152, no. 1–2, pp. 27–47, 2007.
- [74] J. W. Shervias, “Ti–V plots and the petrogenesis of modern and ophiolitic lavas,” *Earth and Planetary Science Letters*, vol. 59, no. 1, pp. 101–118, 1982.
- [75] S. J. Barnes, “The use of metal ratios in prospecting for platinum-group element deposits in mafic and ultramafic intrusions,” *Journal of Geochemical Exploration*, vol. 37, no. 1, pp. 91–99, 1990.
- [76] D. M. Hoatson and R. R. Keays, “Formation of platiniferous sulfide horizons by crystal fractionation and magma mixing in the Munni Munni layered intrusion, West Pilbara Block, Western Australia,” *Economic Geology*, vol. 84, no. 7, pp. 1775–1804, 1989.
- [77] E. Saccani, “A new method of discriminating different types of post-Archean ophiolitic basalts and their tectonic significance using Th–Nb and Ce–Dy–Yb systematics,” *Geoscience Frontiers*, vol. 6, no. 4, pp. 481–501, 2015.
- [78] M. Maffione, C. Thieulot, D. J. J. van Hinsbergen, A. Morris, O. Plümper, and W. Spakman, “Dynamics of intraoceanic subduction initiation: 1. Oceanic detachment fault inversion and the formation of supra-subduction zone ophiolites,” *Geochemistry, Geophysics, Geosystems*, vol. 16, no. 6, pp. 1753–1770, 2015.
- [79] J. F. Lebrun, G. D. Karner, and J. Y. Collot, “Fracture zone subduction and reactivation across the Puysegur ridge/trench system, southern New Zealand,” *Journal of Geophysical Research: Solid Earth*, vol. 103, no. B4, pp. 7293–7313, 1998.
- [80] R. J. Stern, “Subduction initiation: spontaneous and induced,” *Earth and Planetary Science Letters*, vol. 226, no. 3–4, pp. 275–292, 2004.
- [81] D. Arcay, S. Lallemand, S. Abecassis, and F. Garel, “Can subduction initiation at a transform fault be spontaneous?,” *Solid Earth*, vol. 11, no. 1, pp. 37–62, 2020.
- [82] T. E. Keenan, J. Encarnación, R. Buchwaldt et al., “Rapid conversion of an oceanic spreading center to a subduction zone inferred from high-precision geochronology,” *Proceedings of the National Academy of Sciences of the United States of America*, vol. 113, no. 47, pp. E7359–E7366, 2016.
- [83] B. Maunder, J. Prytulak, S. Goes, and M. Reagan, “Rapid subduction initiation and magmatism in the Western Pacific driven by internal vertical forces,” *Nature communications*, vol. 11, no. 1, p. 1874, 2020.
- [84] M. Baes, S. V. Sobolev, and J. Quinteros, “Subduction initiation in mid-ocean induced by mantle suction flow,” *Geophysical Journal International*, vol. 215, no. 3, pp. 1515–1522, 2018.
- [85] E. Carter, B. O’Driscoll, R. Burgess, and P. Clay, “Multi-stage fluid infiltration and metasomatism in supra-subduction zone mantle: evidence from halogens and noble gases in the Leka Ophiolite Complex, Norway,” *Geochimica et Cosmochimica Acta*, vol. 307, pp. 258–280, 2021.
- [86] P. F. Zhang, M. F. Zhou, and G. P. Yumul Jr., “Coexistence of high-Al and high-Cr chromite orebodies in the Acoje block of the Zambales ophiolite, Philippines: evidence for subduction initiation,” *Ore Geology Reviews*, vol. 126, article 103739, 2020.
- [87] Y. Niu, “Mantle melting and melt extraction processes beneath ocean ridges: evidence from abyssal peridotites,” *Journal of Petrology*, vol. 38, no. 8, pp. 1047–1074, 1997.
- [88] J. M. Warren, “Global variations in abyssal peridotite compositions,” *Lithos*, vol. 248, pp. 193–219, 2016.
- [89] H. Paulick, W. Bach, M. Godard, J. C. M. de Hoog, G. Suhr, and J. Harvey, “Geochemistry of abyssal peridotites (Mid-Atlantic Ridge, 15°20’N, ODP Leg 209): Implications for fluid/rock interaction in slow spreading environments,” *Chemical Geology*, vol. 234, no. 3–4, pp. 179–210, 2006.
- [90] A. Verencar, A. Saha, S. Ganguly, and C. Manikyamba, “Tectono-magmatic evolution of Tethyan oceanic lithosphere in supra subduction zone fore arc regime: Geochemical fingerprints from crust-mantle sections of Naga Hills Ophiolite,” *Geoscience Frontiers*, vol. 12, no. 3, article 101096, 2021.
- [91] S. S. Chen, R. Gao, Z. Wang, T. Hou, J. Liao, and C. Yan, “Coexistence of Hainan plume and stagnant slab in the mantle

transition zone beneath the South China Sea spreading ridge: constraints from volcanic glasses and seismic tomography,” *Lithosphere*, vol. 2, article 6619463, 2021.

- [92] T. J. Falloon and L. V. Danyushevsky, “Melting of refractory mantle at 1.5, 2 and 2.5 GPa under anhydrous and H₂O-undersaturated conditions: implications for the petrogenesis of high-Ca boninites and the influence of subduction components on mantle melting,” *Journal of Petrology*, vol. 41, no. 2, pp. 257–283, 2000.
- [93] C. Manikyamba, J. Ray, S. Ganguly et al., “Boninitic metavolcanic rocks and island arc tholeiites from the Older Metamorphic Group (OMG) of Singhbhum Craton, eastern India: geochemical evidence for Archean subduction processes,” *Precambrian Research*, vol. 271, pp. 138–159, 2015.